# Isotopic Resolution of Fission Fragments from 238U+12C Transfer and Fusion Reactions

M. Caamano, F. Rejmund, X. Derkx, K.-H. Schmidt, L. Andouin, C.-O. Bacri, G. Barreau, J. Benlliure, E. Casarejos, B. Fernández-Domínguez, et al.

# Isotopic Resolution of Fission Fragments from $^{238}$U+$^{12}$C Transfer and Fusion Reactions

M. Caamaño[1 *], F. Rejmund[*], X. Derkx[*], K.-H. Schmidt[*], L. Andouin[†], C.-O. Bacri[†], G. Barreau[**], J. Benlliure[‡], E. Casarejos[‡], B. Fernández-Domínguez[2 §], L. Gaudefroy[¶], C. Golabek[*], B. Jurado[**], A. Lemasson[*], A. Navin[*], M. Rejmund[*], T. Roger[*], A. Shrivastava[*], C. Schmitt[*] and J. Taieb[¶]

[*]*GANIL, CEA/DSM-CNRS/IN2P3, BP 55027, F-14076 Caen cedex 5, France*
[†]*IPN Orsay, IN2P3/CNRS-UPS, Georges Clemenceau 15 91406 Orsay, France*
[**]*CENBG, IN2P3/CNRS-UB1, 33175 Gradignan cedex, France*
[‡]*Universidade de Santiago de Compostela, E-15706 Santiago de Compostela, Spain*
[§]*University of Liverpool, Liverpool L69 7ZE, United Kingdom*
[¶]*CEA/DAM Île-de-France, BP 12 91680 Bruyères-le-Châtel, France*

**Abstract.** Recent results from an experiment at GANIL, performed to investigate the main properties of fission-fragment yields and energy distributions in different fissioning nuclei as a function of the excitation energy, in a neutron-rich region of actinides, are presented. Transfer reactions in inverse kinematics between a $^{238}$U beam and a $^{12}$C target produced different actinides, within a range of excitation energy below 30 MeV. These fissioning nuclei are identified by detecting the target-like recoil, and their kinetic and excitation energy are determined from the reconstruction of the transfer reaction. The large-acceptance spectrometer VAMOS was used to identify the mass, atomic number and charge state of the fission fragments in flight. As a result, the characteristics of the fission-fragment isotopic distributions of a variety of neutron-rich actinides are observed for the first time over the complete range of fission fragments.

**Keywords:** neutron-rich actinides, transfer-induced fission, fragment identification, inverse kinematics
**PACS:** 24.75.+i,24.87.+y,25.70.Jj,25.70.Hi

## INTRODUCTION

Fission produces the largest collective motion of nucleons inside the nucleus, while, at the same time, is also strongly influenced by the structure of the fissioning nucleus. At low excitation energy, shell structure and pairing correlations mark the main features of the fragment distribution. It is well-known that the fission-fragment mass distribution of most actinides in the range of masses from 230 to 256 are characterized by two or even three-humped shapes. This feature has been understood as a superposition of independent fission modes [1, 2] corresponding to different paths in the potential surface of the fission process [2, 3]. The average mass of the heavy fragment was observed to remain

---

[1] Present address: Universidade de Santiago de Compostela, E-15706 Santiago de Compostela, Spain
[2] Present address: GANIL, CEA/DSM-CNRS/IN2P3, BP 55027, F-14076 Caen cedex 5, France

constant around $A \sim 140$ in spontaneous and neutron-induced fission [3]. Similarly, campaigns of fusion-fission experiments showed a constant heavy-fragment average mass at $A \sim 132$ and $A \sim 140$ [4]. These experimental results are well described with a symmetric and two asymmetric fission channels, the asymmetric modes being commonly associated with spherical and deformed neutron shells in $N = 82$ and $N \sim 84 - 90$ [4]. Recently, the study of fragment atomic-number distribution in low-energy fission of neutron-deficient actinides showed the heavy fragment distribution centered on $Z \approx 54$, independently of the fissioning system [5]. A detailed analysis of these data showed the two asymmetric modes being centered on $Z \sim 53$ and $Z \sim 55$, for all identified actinides [6]. These results are somehow surprising when compared with the neutron-shell influence described above, for which a change of the average atomic number of the heavy fragment with the mass of the fissioning system was expected. The controversy between the independent measurements of fragment mass and atomic number sets a challenge on the theoretical description of fission, and namely on what drives the process. The existence of systematic measurements of fission characteristics over a broad range of fissioning systems is very important to constraint the different models. Nonetheless, as different quantities were measured in different sets of data (fission-fragment mass in direct kinematics, or atomic number in the case of inverse-kinematics experiments), the simultaneous measurement of both mass and atomic number of fragments is imperatively required to go further. Unfortunately, information on full isotopic-fragment distributions is very scarce; it mainly consists of thermal neutron-induced fission of a limited number of actinides [7, 8, 9, 10, 11, 12, 13, 14, 15], and is restricted to the light fragments, due to technical difficulties in identifying high-$Z$ products in direct kinematics. The isotopic distribution of the heaviest fragment can be determined using radio-chemical techniques [16, 17], but with poor precision and in a reduced range of the total production.

Another important characteristic of low-energy fission in even-$Z$ nuclei is the enhanced production of fragments with an even number of protons. This has been interpreted as a signature that completely-paired proton configurations are preserved up to the scission point [13, 18]. The difference between even and odd element yields may be related to the heating of the nucleus undergoing fission on its way to the scission point, and hence to the viscosity of cold nuclear matter. Experimentally, the even-odd staggering has been observed to depend strongly on the fissility of the fissioning nucleus [8], its excitation energy [19], and the fragment distribution asymmetry [11, 14, 20]. As discussed in these proceedings[21], the recent results with inverse kinematics show that the dependence of the even-odd effect with fissility is strongly affected by the asymmetry of the fission-fragment distribution, and puts forward a dissipated energy independent of fissility. These results show the need for more precise information on isotopic-yield distributions at symmetry, and for wider systematics than the present ones.

The points discussed above indicate that a deeper insight into fission dynamics can only be gained with a systematic and simultaneous measurement of complete mass and atomic number distributions of fission fragments. This is the aim of the present work, based on multi-nucleon transfer-induced fission in inverse kinematics with the VAMOS spectrometer [22] at GANIL. In addition, and in order to continue the systematic study of neutron-deficient actinides at GSI, the present experiment focus on the production of fissioning actinides in the neutron-rich region.

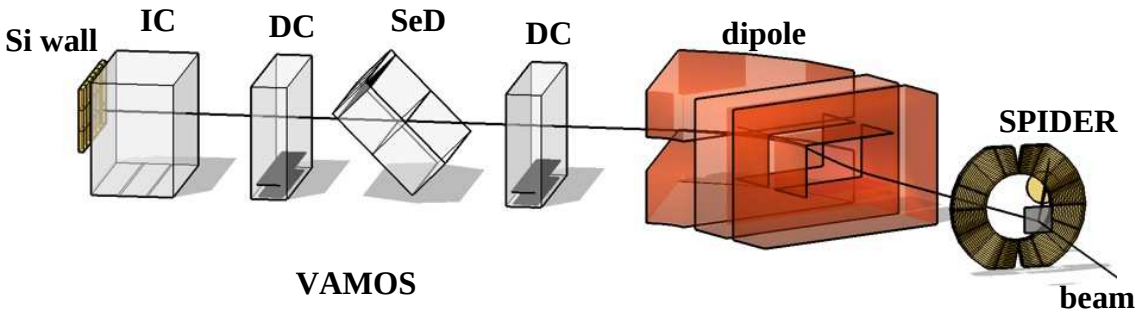


**FIGURE 1.** Experimental set-up. The VAMOS spectrometer and associated detectors are depicted in the figure. The dE-E telescope SPIDER is placed between the target (in grey) and the magnets of the spectrometer (in red)

## MULTI-NUCLEON TRANSFER-INDUCED FISSION OF $^{238}$U IN INVERSE KINEMATICS

The experiment aimed to produce different fissioning systems by multi-nucleon transfer reactions between a 6.1 MeV/u $^{238}$U beam and a 100 $\mu$g/cm$^2$ $^{12}$C target. The resulting systems cover a region of neutron-rich actinides, from U to Cm. The beam energy was chosen as a compromise between the fission production, the geometry of detection, and the opening of other reaction channels. At this energy, around 10% above the Coulomb barrier, a total fission cross-section around 300 mb was previously measured for $^{12}$C+$^{232}$Th, with a total transfer-fission probability ten times lower than fusion-fission [23]. A similar cross-section is expected for the present reaction. Different fissioning systems are produced from the interaction of the U beam and the carbon target: inelastic collisions provide a range of excitation energy to the $^{238}$U beam, while transfer reactions produce a collection actinides, always in a range of excitation energy below 30 MeV. In addition, fusion reactions produce fission of $^{250}$Cf with $\sim$40 MeV of excitation energy. The compound systems are expected to have angular momenta lower than 20 $\hbar$. The fission fragments produced will cover a wide range of energy (2-10 MeV/u), mass (90-150), atomic number (30-60), and charge states ($\sim$10 charges per isotope). Inverse kinematics of in-flight fission at 6.1 MeV/u confines the angular distribution of the fragments in a cone of about 25 deg in laboratory frame.

### Experimental set-up

The kinematics reconstruction of the direct reactions (inelastic scattering and multi-nucleon transfer) allows the identification of the resulting fissioning systems, along with an estimation of their excitation energy. In addition, the characteristics of in-flight fission in inverse kinematics make the detection of the complete fragment distribution possible.

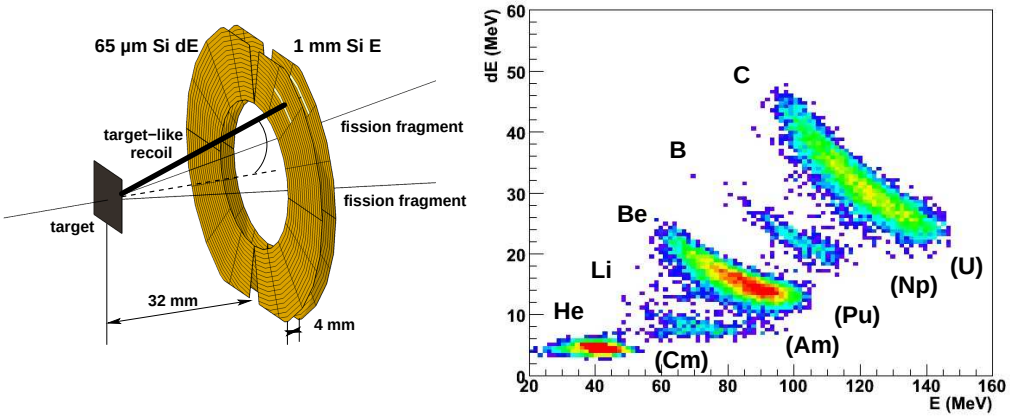


**FIGURE 2.** Left panel: Schematic drawing of the SPIDER-detector ensemble. Right Panel: Identification of target-like recoil in SPIDER. Correlation between dE-E shows the different recoil species produced in inelastic and transfer reactions. The corresponding fissioning elements are indicated in parenthesis.

These tasks are performed by two dedicated detection systems: the dE-E SPIDER telescope, and the VAMOS spectrometer (see Fig. 1).

SPIDER (Silicon Particle Identification DEtector Ring) is used to detect and identify the target-like recoils, and to reconstruct the kinematics of transfer reactions. It consists of two annular silicon detectors (see Fig. 2). Both are 48 mm radius double-sided detectors with an inner hole of 24 mm radius. They are segmented into 16 rings of 1.5 mm radius in one side, and 16 sectors in the other. The first detector, used to measured energy loss (dE), is 65 $\mu$m thick, while the second one, for residual energy ($E_{res}$), is 1 mm thick. The two detectors are placed 32 mm after the target, with a separation of 4 mm between them. The SPIDER ensemble detects and identifies the target-like recoil by means of dE-E correlation (being E=dE+$E_{res}$). The reconstruction of direct kinematics is done with the total energy measurement and the determination of the recoil angle. The segmentation of the detectors allows the measurement of the recoil angle with $\sim$1 deg of geometrical uncertainty; depending on the reaction, this is translated in $\sim$2 MeV of excitation-energy resolution, in both the recoil and the fissioning system. Figure 2 shows the dE-E correlation with the identification of the different recoil species. Recoil identification resulted in the detection of C, B, Be, Li and He. Despite the isotopic identification of the target-like recoil is not achieved, the most probable channels may be estimated from the $Q_{gg}$ values [24]. These correspond to $^{238}$U, $^{239}$Np, $^{240}$Pu, and $^{243}$Am as fissioning systems, respectively. In addition, fusion-fission reactions are identified by the absence of target-like recoil.

The fission fragments pass through the inner hole of SPIDER, and are identified in the VAMOS spectrometer and its associated detectors (see Fig. 1). The whole spectrometer can be rotated around the target to cover a specific angular region. In this case, VAMOS is rotated by 20 deg in order to cover the angular region with largest fragment production, close to the edge of the fission cone. This configuration allows the detection of, at most, one of the two fragments per fission. In this experiment, the geometrical acceptance of VAMOS is $\sim$14 deg in the horizontal plane, and $\sim$3 deg in the vertical plane; the detection area accepts particles within $\pm$10 % of the central magnetic rigidity. In order

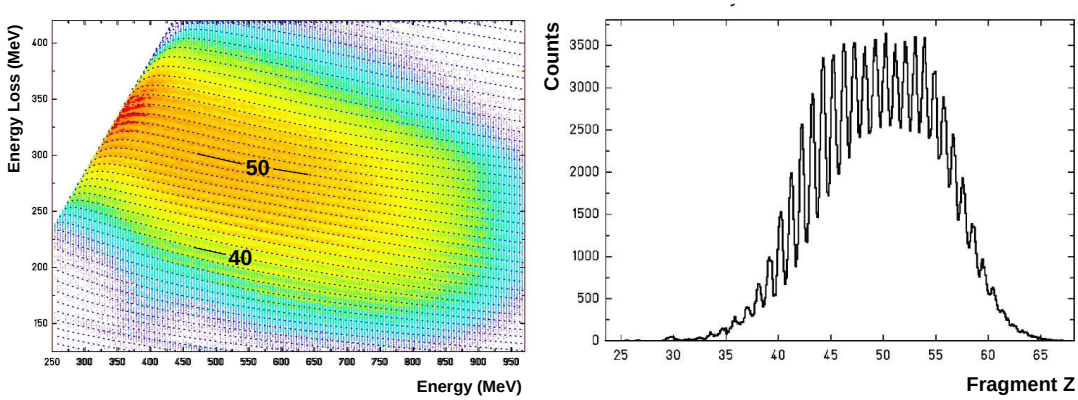


**FIGURE 3.** Fragment-$Z$ identification in VAMOS. Left panel: dE-E correlation. The dashed lines correspond to the analytical description of dE-E correlation for each $Z$. Right panel: $Z$ projection along the analytical lines. The shape of the distribution is due to the addition of different sets of data not yet normalized.

to cover the most of the momentum and charge-state distributions, different values of the central magnetic rigidity were used during the experiment. Finally, the ensemble of the different magnetic settings covers from 1.010 to 1.360 Tm of magnetic rigidity. The detection area in VAMOS consisted of two Drift Chambers (DC) to measure particle positions and angles, a Secondary-electron Detector (SeD) to measure the time of flight, an Ionization Chamber (IC) to measure energy loss, and a wall of twenty-one Silicon detectors to measure the residual energy of the particle (see [25] for more details on the detectors). In addition, two clovers of the Germanium-array EXOGAM [26] were placed around the target to identify nuclear levels in the fission fragments.

## Isotopic identification of fission fragments

The information obtained by the detectors in VAMOS allows a complete identification of the fission fragments in mass ($A$), atomic number ($Z$), charge state ($q$), and kinetic energy ($KE$). In addition, the ion-optical reconstruction gives angular information of the fragment at the target position (before entering VAMOS). The total energy of the particle is the sum of the energy loss in the IC and the residual energy measured in the Si wall. In addition, estimations of energy losses in the target, windows of detectors, etc. is also added. The dE-E correlation allows to separate the different $Z$ detected in VAMOS, as seen in Fig. 3. Around thirty different species, over a range of more than 600 MeV, are observed. At low energy, the slope of the lines changes due to the Bragg peak produced by low-energy particles stopping in the IC. The lines in Fig. 3 are the result of an analytical approach to describe the dE-E behaviour. In this approach, the energy-loss dE depends on the velocity of the particle, and on an effective charge. The latter depends on the $Z$ of the particle, and also on the velocity. In addition, corrections due to electron-shell closure are taken into account. This analytical description allows to assign a $Z$ to individual events. The resolution, along the whole energy range, is $\Delta Z/Z \approx 1.5 \cdot 10^{-2}$.

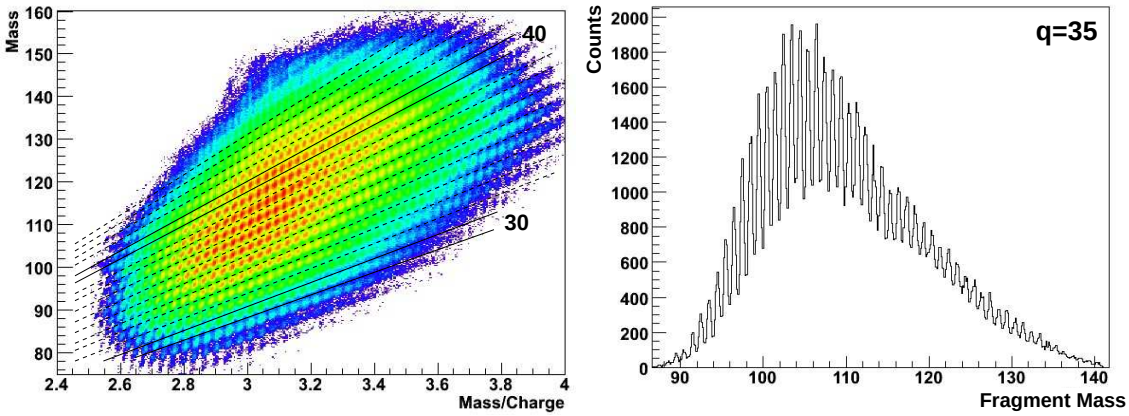


**FIGURE 4.** Fragment-$A$ identification in VAMOS. Left panel: $A$-$A/q$ correlation. The dashed lines separate $A$-$A/q$ groups of fragments with the same charge state $q$. Right panel: $A$ distribution of a single $q$. The distribution is obtained with $A = q \times A/q$. The shape of the distribution is due to the addition of different sets of data not yet normalized.

Horizontal and vertical positions measured in the two DCs are used to determine the total path from the target, the magnetic rigidity (B$\rho$), and the scattering angle of the particle in laboratory frame. This is done by mapping all possible trajectories along the spectrometer, as a function of B$\rho$, angle and position of the particle (more details can be found in [25]). The time of flight, calculated between the SeD and the high frequency of the cyclotron, is combined with the reconstructed path to obtain the velocity. The mass of the fragments is measured, in a first step, with their total energy and velocity. The reconstructed B$\rho$ and velocity are used to determined the $A/q$ ratio. Figure 4 shows the relation $A$ vs. $A/q$, where the different fragments can be identified in mass and charge state. The $A$ identification is done in a second step that takes profit from the better resolution in $A/q$: fragments with the same $q$ form the diagonal lines shown in Fig. 4; the final $A$ identification is obtained multiplying the $A/q$ of systems contained in the same diagonal by the corresponding $q$. This procedure allows the identification of more than 70 masses, from $A \approx 80$ to 150, with a resolution of $\Delta A/A \approx 0.6 \cdot 10^{-2}$ (see Fig. 4). The mass resolution in this experiment was limited by the time of flight measurement, with 1 ns of resolution over $\sim$170 ns of time of flight.

In addition, the correlation between the nuclear levels identified with the EXOGAM detectors, and the isotopic identification obtained in the spectrometer allows to assure the unambiguous assignment of $Z$, $A$ and $q$ for all fragments detected in VAMOS.

## CONCLUSIONS AND PERSPECTIVES

The data analysis of the experiment is currently in its initial stages, however, some important achievements can already be highlighted. Multi-nucleon transfer reactions between $^{238}$U and $^{12}$C produced a range of fissioning nuclei between U and Cm, already identified by dE-E correlation. In addition, fusion-fission reactions allowed to include $^{250}$Cf in the collection of fissioning nuclei to study.

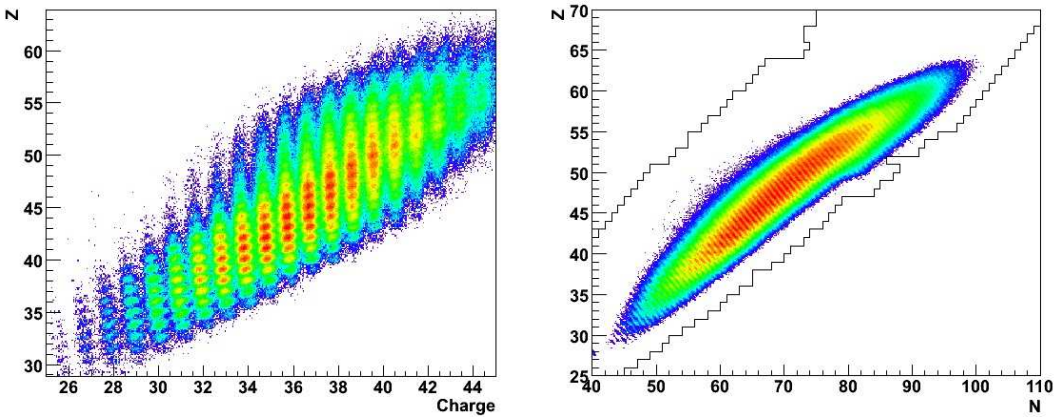


**FIGURE 5.** Atomic number $Z$ versus charge-state $q$ (left), and versus neutron number $N$ (right) for the whole fission-fragment production in this experiment. The limits of observed isotopes are shown for reference in the right panel.

The measurement of fission fragments in inverse kinematics using the VAMOS spectrometer allowed, for the first time in a single experiment, the complete characterization of the whole distribution of fission fragments along with the fissioning system. More than 300 isotopes are identified in mass, atomic number, and charge state (see Fig. 5). The kinematic properties of the fragments are also determined by measuring the kinetic energy and angle of fragments. These results show already the power of the present experimental approach, resulting in the most complete experimental characterization of fission in minor actinides so far.

The next steps of the analysis will concern the determination of fission fragment isotopic yields, by normalising the different dipole settings in order to reconstruct the velocity distribution as well as the $q$-state distribution for each of the ($Z$,$A$) fragment. Energy spectra, and angular distributions will also derive from these results. For the first time, correlations between these observables will be possible, revealing shell effects, and the proton or neutron influence in the fission process. Also, even-odd staggering either in protons and neutrons can be explored in the whole fragment distribution. Finally, these features of fragments distribution are to be explored as a function of the entrance channel, *i.e.* the fissioning system and its excitation energy.

## ACKNOWLEDGMENTS

This work has been supported by Région Basse Normandie with a Chair of Excellence position in GANIL, as well as by the EURATOM programme under the contract number 44816.

## REFERENCES

1. A. Turkevich, and J. B. Niday, *Phys. Rev.* **84**, 52 (1951).
2. A. Brosa, and A. Müller, *Phys. Rep.* **197**, 167 (1990).
3. K. F. Flynn, et al., *Phys. Rev. C* **5**, 1725 (1972), and references therein.
4. M. G. Itkis, et al., *Dynamics at the Extreme 2000, Dubna* (2000).

5. K.-H. Schmidt, et al., *Nucl. Phys. A* **665**, 221 (2001).
6. C. Böcktiegel, et al., *Nucl. Phys. A* **802**, 12 (2008).
7. G. Siegert, et al., *Phys. Rev. C* **14**, 1864 (1976).
8. W. Lang, et al., *Nucl. Phys. A* **345**, 34 (1980).
9. C. Schmitt, et al., *Nucl. Phys. A* **430**, 21 (1984).
10. U. Quade, et al., *Nucl. Phys. A* **487**, 1 (1988).
11. J. L. Sida, et al., *Nucl. Phys. A* **502**, 233 (1989).
12. M. Djebara, et al., *Nucl. Phys. A* **496**, 346 (1989).
13. J.-P. Bocquet, and R. Brissot, *Nucl. Phys. A* **502**, 213 (1989).
14. R. Hentzschel, et al., *Nucl. Phys. A* **571**, 427 (1994).
15. I. Tsekhanovich, et al., *Nucl. Phys. A* **688**, 633 (2001).
16. I. Nishinaka, et al., *Phys. Rev. C* **56**, 891 (1997).
17. R. Tripathi, et al., *Phys. Rev. C* **69**, 024613 (2004).
18. F. Rejmund, A. V. Ignatyuk, A. R. Junghans, and K.-H. Schmidt, *Nucl. Phys. A* **678**, 215 (2000).
19. S. Steinhäuser, *Untersuchung der Elementausbeuten in der Niederenergiespaltung neutronenarmer radioaktiver Kerne*, Ph.D. thesis, Institut für Kernphysik, Technische Universität Darmstadt (1997).
20. D. Rochman, et al., *Nucl. Phys. A* **735**, 3 (2004).
21. M. Caamaño, F. Rejmund, and K.-H. Schmidt, *These proceedings* (2009).
22. H. Savajols, et al., *Nucl. Inst. and Meth. B* **204**, 146 (2003).
23. D. C. Biswas, et al., *Phys. Rev. C* **56**, 1926 (1997).
24. J. S. Karp, S. Steadman, S. Gazes, and R. Ledoux, *Phys. Rev. C* **25**, 1838 (1982).
25. S. Pullanhiotan, et al., *Nucl. Inst. and Meth. A* **593**, 343 (2008).
26. J. Simpson, et al., *Acta Phys. Hung., New Series, Heavy Ion Physics* **11**, 159 (2000).